Atmos. Chem. Phys. Discuss., doi:10.5194/acp-2016-716, 2016
Manuscript under review for journal Atmos. Chem. Phys.
Published: 10 August 2016


Atmospheric Chemistry and Physics Discussions

# OH reactivity at a rural site (Wangdu) in the North China Plain: Contributions from OH reactants and experimental OH budget

Hendrik Fuchs[1], Zhaofeng Tan[2], Keding Lu[2], Birger Bohn[1], Sebastian Broch[1], Steven S. Brown[3], Huabin Dong[2], Sebastian Gomm[1,a], Rolf Häseler[1], Lingyan He[4], Andreas Hofzumahaus[1], Frank Holland[1], Xin Li[1,b], Ying Liu[2], Sihua Lu[2], Kyung-Eun Min[3,5,c], Franz Rohrer[1], Min Shao[2], Baolin Wang[2], Ming Wang[6], Yusheng Wu[2], Limin Zeng[2], Yingson Zhang[2], Andreas Wahner[1], and Yuanhang Zhang[2,7]

[1]Institute of Energy and Climate Research, IEK-8: Troposphere, Forschungszentrum Jülich GmbH, Jülich, Germany
[2]College of Environmental Sciences and Engineering, Peking University, Beijing, China
[3]Chemical Sciences Division, Earth System Research Laboratory, National Oceanic and Atmospheric Administration, Boulder, CO, USA
[4]Key Laboratory for Urban Habitat Environmental Science and Technology, School of Environment and Energy, Peking University Shenzhen Graduate School, Shenzhen, China
[5]Cooperative Institute for Research in Environmental Sciences, University of Colorado, Boulder, CO, USA
[6]School of Environmental Sciences and Engineering, Nanjing University of Information Science and Technology, Nanjing, China
[7]Innovation Excellence Center for Urban Atmospheric Environment of Chinese Academy of Sciences, China
[a]now at: d-fine GmbH, Opernplatz 2, 60313 Frankfurt, Germany
[b]now at: College of Environmental Sciences and Engineering, Peking University, Beijing, China
[c]now at: School of Environmental Science and Engineering, Gwangju Institute of Science and Technology, Gwangju, Korea

*Correspondence to:* H. Fuchs (h.fuchs@fz-juelich.de), Y. Zhang (yhzhang@pku.edu.cn)

**Abstract.** In 2014, a large, comprehensive field campaign was conducted in the densely populated North China Plain. The measurement site was located in a botanic garden close to the smaller town Wangdu without major industry, but influenced by regional transportation of air pollution. The loss rate coefficient of atmospheric hydroxyl radicals (OH) was quantified by direct measurements of the OH reactivity. Values ranged between 10 and 20 $s^{-1}$ for most of the daytime. Highest values were reached in the late night with maximum values around 40 $s^{-1}$. OH reactants mainly originated from anthropogenic activities as indicated (1) by a good correlation between measured OH reactivity and carbon monoxide, and (2) by a high contribution of nitrogen oxide species to the OH reactivity. Measured total OH reactivities can be well explained by measured trace gas concentrations including organic compounds, oxygenated organic compounds, CO and nitrogen oxides. Significant, unexplained OH reactivity was only observed during nights, when biomass burning of agricultural waste occurred on surrounding fields. OH reactivity measurements also allow investigating the chemical

Atmos. Chem. Phys. Discuss., doi:10.5194/acp-2016-716, 2016
Manuscript under review for journal Atmos. Chem. Phys.
Published: 10 August 2016


Atmospheric Chemistry and Physics Discussions

OH budget. During this campaign, the OH destruction rate calculated from measured OH reactivity and measured OH concentration was balanced by the sum of OH production from ozone and nitrous acid photolysis and OH regeneration from hydroperoxyl radicals within the uncertainty of measurements. However, also a tendency for higher OH destruction compared to OH production at lower concentrations of nitric oxide is observed consistent with previous findings in field campaigns in China.

Atmos. Chem. Phys. Discuss., doi:10.5194/acp-2016-716, 2016
Manuscript under review for journal Atmos. Chem. Phys.
Published: 10 August 2016


Atmospheric Chemistry and Physics Discussions

## 1 Introduction

Hydroxyl radicals (OH) are the most important oxidization agent for inorganic and organic pollutants in the atmosphere (Ehhalt, 1999). A large number of field campaigns have been conducted in the past to improve our understanding of radical chemistry in the atmosphere at various locations all over the world. However, only few have taken place in China, where air pollution is still a severe problem (Lu et al., 2010). Measurements during field campaigns in the Pearl-River-Delta (PRD) and at a suburban location south of Beijing (Yufa) revealed a lack of understanding of radical chemistry by state-of-the-art chemical models pointing to unknown OH radical sources (Hofzumahaus et al., 2009; Lu et al., 2012, 2013). Similar results were found at other locations, which were mainly dominated by biogenic emissions (Rohrer et al., 2014).

In summer 2014, the effort to improve our knowledge of radical chemistry in Chinese megacity areas was continued by a comprehensive field campaign at a location close to the city Wangdu in the North China Plain south-west of Beijing (Tan et al., 2016). A large set of instruments was deployed to detect radicals (OH, $HO_2$, $RO_2$), reactive trace gases (e.g., CO, $NO_x$, volatile organic compounds (VOC)) and aerosols properties. Whereas time series of radical measurements and a comparison with results from a chemical box model calculation are discussed in our accompanying paper by Tan et al. (2016), the discussion here focusses on the analysis of measured OH reactivity.

OH reactivity ($k_{OH}$) is the pseudo-first order loss rate coefficient of OH radicals and represents the inverse chemical lifetime of OH.

$$k_{OH} = \sum_i k_{OH+Xi}[X_i] \quad (1)$$

$X_i$ represents any OH reactant. Because of the large number of OH reactants in the atmosphere, it is of high value for the interpretation of radical chemistry to compare the direct measurement of $k_{OH}$ with reactivities calculated from measured atmospheric OH reactant concentrations.

Depending on the instrumentation that were available in field campaigns in the past, up to more than 70 % of the measured reactivity was found to remain unexplained in different types of environments (e.g., cities, forests) (Yang et al., 2016). For our previous field campaigns in China, the measured OH reactivity was two times larger than the calculated $k_{OH}$. The discrepancy could be quantitatively explained by the reactivity from oxygenated VOCs (OVOC), which were not measured, but estimated by a chemical model (Lou et al., 2010; Lu et al., 2013). In this campaign, the number of measured species was extended and included important atmospheric OVOCs, for example formaldehyde, acetaldehyde, isoprene oxidation products, and glyoxal.

Measurements of OH reactivity and OH concentrations can be combined to calculate the loss rate of OH radicals. This can then be compared to the sum of OH production rates from ozone and nitrous acid photolysis and reaction of hydroperoxyl radicals with nitric oxide. All quantities that are required to do this calculation were measured in this campaign. This allows for a model-independent

Atmos. Chem. Phys. Discuss., doi:10.5194/acp-2016-716, 2016
Manuscript under review for journal Atmos. Chem. Phys.
Published: 10 August 2016


Atmospheric Chemistry and Physics Discussions

analysis of the chemical OH budget. This approach was successfully applied to quantify unaccounted OH production in our field campaigns in China in 2006 (Hofzumahaus et al., 2009).

In the following, we describe the technique for OH reactivity measurements applied in the campaign in Wangdu, discuss the time series of measurements, compare OH reactivity measurements with calculations from single reactant measurements and analyze the OH budget.

## 2 Experimental

The instruments, their setup at the field site and the measurement conditions are described in Tan et al. (2016). Therefore, only a brief description is given here.

### 2.1 Measurement site

Measurements took place inside a botanic garden close to the small town Wangdu in China between 7 June and 8 July 2014. Wangdu is located in the densely populated North-China Plain, but does not have major industry itself. Major cities are located mainly in the sector from north-east to south-west from Wangdu, whereas there is a mountainous area with less industry north-west of Wangdu. The closest large city is Baoding 35 km north-east of Wangdu. The measurement site had a distance of 2 km from a road with only local traffic. The botanic garden was surrounded by agricultural fields. Trace gases from local biogenic emissions of trees, bushes and from farming may have been present.

Instruments were housed in seven sea containers, which were partly stacked up, so that inlets of instruments were at a height of 7 m above the ground.

### 2.2 Instrumentation

A large number of instruments characterized meteorological conditions, trace gas concentrations and aerosol properties. The measurements used for the OH reactivity analysis are listed in Table 1.

OH and $HO_2$ radical concentrations were measured by a newly built instrument applying laser-induced fluorescence technique (PKU-LIF) (Tan et al., 2016). This instrument detects OH fluorescence by time-delayed single photon counting after excitation by short laser pulses at 308 nm in a low-pressure cell (Holland et al., 2003; Fuchs et al., 2011). $HO_2$ radicals are detected as the sum of OH and $HO_2$ ($=HO_x$) after chemical conversion to OH in the reaction with nitric oxide (NO). In order to avoid significant simultaneous conversion of organic peroxy radicals ($RO_2$) (Fuchs et al., 2011), the amount of NO was adjusted to yield a conversion efficiency of only 6 %.

A commercial cavity ring-down instrument (Picarro model G2401) monitored CO, $CH_4$ and $H_2O$ concentrations. Concentration measurements of ozone by two commercial UV absorption instruments (Environment S.A. model 41M; Thermo Electron model 49i) well agreed during the campaign. Nitrogen monoxide was also detected by several instruments applying chemiluminescence technique. The agreement was on average 20 %. Measurements from one of the instruments ap-

Atmos. Chem. Phys. Discuss., doi:10.5194/acp-2016-716, 2016
Manuscript under review for journal Atmos. Chem. Phys.
Published: 10 August 2016


Atmospheric Chemistry and Physics Discussions

peared to be more precise and are taken here (see Tan et al. (2016) for details). Because the reason for the disagreement could not be identified, the 20 % difference adds to the uncertainty of NO measurements here. Nitrous acid (HONO) concentrations were simultaneously measured by several instruments applying different measurement techniques. The agreement between instruments was diverse. For the purpose of the analysis here, measurements by the well-established LOPAP instrument (long-path absorption photometry) from Forschungszentrum Jülich are used (Li et al., 2014). The choice of the HONO data set has a rather small impact on the results.

For the analysis of the OH reactivity, measurements of organic trace gases are essential. $C_2$-$C_{11}$ alkanes, $C_2$-$C_6$ alkenes, $C_6$-$C_{10}$ aromatics, and isoprene were detected by a home-built gas-chromatography system equipped with a flame ionization detector (FID) (Wang et al., 2014). Formaldehyde (HCHO) was detected by a commercial Hantzsch monitor (Aerolaser model AL4021) and gyloxal (CHOCHO) by a custom-built cavity enhanced spectrometer (Min et al., 2016). In addition, acetaldehyde and the sum of methyl vinyl ketone (MVK) and methacrolein (MACR) were measured by a commercial proton transfer reaction - mass spectroscopy system (PTR-MS, Ionicon). The PTR-MS also measured part of the same species like the GC system (isoprene, benzene, toluene, styrene, $C_8$-aromatics, $C_9$-aromatics), which during daytime well agreed with measurements by GC (Tan et al., 2016).

### 2.3 OH reactivity measurements

The OH reactivity instrument measures directly pseudo first-order loss rate coefficients (Eq 1) of OH in the ambient air. The measurement is based on artificial OH generation by pulsed laser-flash photolysis (LP) of ozone in ambient air combined with the detection of the temporal OH decay by laser induced fluorescence (LIF). The method was initially developed for field application by Sadanaga et al. (2004) and is applied today by several other groups (Lou et al., 2010; Parker et al., 2011; Stone et al., 2016). The instrument deployed in this campaign is similar to the instrument described in Lou et al. (2010), which was used for measurements in our two field campaigns in 2006 in China. Since then, a second instrument was built specifically for the deployment on a Zeppelin NT airship (Li et al., 2014), but can be operated at ground like in this campaign. Figure 1 gives a schematic representation of the instrument without the pump (Edwards model XDS35i) needed for the operation of the low-pressure LIF cell and without the laser that provides the 308 nm radiation for the excitation of OH. The 308 nm radiation is delivered by the dye laser system that is also used in the instrument for the OH $HO_2$, and $RO_2$ concentration measurements described in Tan et al. (2016). This laser has three output fibers to provide laser light, one of which is used for the OH reactivity instrument.

The $k_{OH}$ instrument is mounted in a 19" rack that was placed inside one of the upper sea containers at the field site. The inlet line (outer diameter 10 mm, length approximately 6 m) was made of stainless steel that had a SilcoNert 200 coating. Approximately 20 Liter/min of ambient air is

Atmos. Chem. Phys. Discuss., doi:10.5194/acp-2016-716, 2016
Manuscript under review for journal Atmos. Chem. Phys.
Published: 10 August 2016


Atmospheric Chemistry and Physics Discussions

sampled through a flow-tube made of anodized aluminium (length: 60 cm, inner diameter: 4 cm). Downstream of the flow tube, the flow rate is measured by a flow-meter and controlled by a blower. The pressure inside the flow tube is 1 atm and the temperature was the same as in the field container (between 22 and 30 °C). High OH concentrations on the order of $10^9$ cm$^{-3}$ are produced by flash photolysis of $O_3$ at 266 nm with subsequent reaction of $O^1D$ with water vapor. The 266 nm laser pulses (pulse energy 20 to 28 mJ, repetition rate 1 Hz, pulse duration less than 10 ns) are provided by a compact, frequency quadrupled Nd:YAG laser (Quantel model Ultra 100). The laser is mounted on one side of an optical rail, on which the flow tube is mounted on the opposite side. The laser beam is widened by an optical telescope to a diameter of 3 cm and guided to the flow tube by two turning mirrors.

Water vapor, temperature and pressure in the flow tube are continuously monitored. Normally, ozone and water vapor concentrations in the sampled ambient air are typically sufficiently high in order to produce high OH concentrations. However, ozone can be depleted during night due to its reaction with nitrogen oxides and by deposition processes. Therefore, a small flow of synthetic air (0.2 Liter/min) that has passed an ozonizer (glass tube of fussed silica with a mercury lamp providing 185 nm radiation) can be added, in order to increase ozone mixing ratios in the flow-tube by 40-50 ppbv. The injection is controlled by a solenoid valve which is automatically opened, if the ozone mixing ratio in ambient air drops below 30 ppbv.

In a distance of 48 cm from the inlet of the flow-tube, 1 Liter/min of the total flow is sampled from the center of the flow tube through a conical nozzle into the OH detection cell. The design of the OH fluorescence cell is the same as used for OH concentration measurements (Tan et al., 2016).

In the cell, OH is excited by 308 nm radiation from a tunable frequency-doubled dye laser, which is operated at a pulse repetition rate of 8.5 kHz. The OH fluorescence is detected by gated photon counting and accumulated in time bins of 0.6 ms. This way, the chemical decay of OH in the flow tube is recorded for 1 s after the photolysis laser pulse. For photon detection, a gated multichannel photomultiplier (Photek, PM325) is used in combination with a multichannel counting card (Sigma Space, AMCS).

In order to achieve sufficiently precise count rates, 60 decay curves are taken for one measurement. Because of the scanning of the laser over the absorption line of OH in order to track slow drifts in the wavelength of laser, the amplitude of the decay curve changes periodically. Therefore, ten OH decay curves are summed up to equalizes the amplitude. Six of the summed curves are then averaged to determine realistic error estimates needed for the fit procedure. A weighted single-exponential fit (Levenberg-Marquardt minimization) is then applied to derive the OH reactivity (Eq. 1). Approximately the first 30 to 50 ms of the decay curve are not included in the fit, because these points deviate from the single-exponential behavior that is observed at later times. The likely reason is that the spatial OH distribution is not perfectly homogeneous near the inlet nozzle of the OH detection cell right after the laser pulse.

Atmos. Chem. Phys. Discuss., doi:10.5194/acp-2016-716, 2016
Manuscript under review for journal Atmos. Chem. Phys.
Published: 10 August 2016


Atmospheric Chemistry and Physics Discussions

Diffusion to the wall of the flow tube, where OH is lost by wall reactions, causes loss of OH even in the absence of OH reactants. This zero loss rate is regularly measured in humidified air (purity 99.999 %). Typical zero loss rates measured in laboratory characterization measurements are around $3\,s^{-1}$ for this instrument. A slightly higher value of $3.8\,s^{-1}$ was derived in measurements sampling synthetic air from a gas cylinder during the campaign. Analysis of the synthetic air in this gas cylinder by gas-chromatography yielded contaminations with an OH reactivity of $0.7\,s^{-1}$. Therefore, an instrumental zero decay value of $3.1\,s^{-1}$ was subtracted from ambient OH reactivity measurements consistent with previous values for this instrument. The reactivity measured in the synthetic air is considered as a potential systematic error of the OH reactivity measurements in this campaign. The accuracy of our LP-LIF technique has been tested with CO and $CH_4$ mixtures in synthetic air. Measured $k_{OH}$ agreed better than 10 % with the expected, calculated OH reactivity for values up to $60\,s^{-1}$ in agreement with previous studies by Lou et al. (2010). At higher $k_{OH}$ values, the initial non-exponential part of the OH decay curve starts to influence the quality of the fitted OH decay curve, but such high $k_{OH}$ values were not encountered in the campaign at Wangdu (Fig. 2).

Potential interferences that could be present in the OH concentration detection would not affect the measured OH reactivity, because OH that would be artificially produced inside the measurement cell would only increase the background signal, but not the decay time as long as it does not change on the time scale of the OH decay measurement (1 s). In any case, however, effects are expected to be negligible due to the high OH concentration inside the flow tube that are much higher compared to ambient OH concentrations, for which interferences have been recognized. This holds for the known interference from ozone photolysis by the 308 nm laser radiation, but also for other potential interferences that have been reported for OH concentration measurements (**??**) and which could not fully excluded for this campaign (Tan et al., 2016).

If ambient NO concentrations are high enough to lead to a significant regeneration of OH from secondarily formed $HO_2$, the shape of the decay curve changes to a bi-exponential behavior. As shown in Lou et al. (2010) no significant effects are expected for NO mixing ratios of up to 20 ppbv for realistic OH reactant mixtures in our instrument. During the campaign in Wangdu, NO mixing ratios were generally well below 20 ppbv and, thus, no bi-exponential behavior was observed. NO mixing ratios exceeded 20 ppbv only for some short periods mainly during nighttime on three days, but measurements still appeared as single exponential decays in these cases.

## 3 Results and Discussion

### 3.1 Time series of OH reactivity

Measured OH reactivity values ranged between 10 and $20\,s^{-1}$ during this campaign for most of the time (Fig. 2). In general, values were lower during daytime than at night. During the first two weeks, midday OH reactivity increased from $10\,s^{-1}$ on 8 June to values higher than $20\,s^{-1}$ between 15

Atmos. Chem. Phys. Discuss., doi:10.5194/acp-2016-716, 2016
Manuscript under review for journal Atmos. Chem. Phys.
Published: 10 August 2016


Atmospheric Chemistry and Physics Discussions

and 19 June. After 19 June, OH reactivity was generally lower and more uniform till the end of the campaign.

Maximum values were observed during nighttime and early morning hours, when OH reactivities show spikes with values of up to $60\,s^{-1}$ for short periods of less than one hour. The high reactivity values were probably caused by emissions into the shallow nocturnal boundary layer. The short duration indicates that nearby local sources were responsible for these events. This happened more frequently during the first part of the campaign and only few spikes were observed after 19 June.

The overall changes in OH reactivity values from day to day were likely dominated by anthropogenic activities during this campaign. Total OH reactivity measurements were correlated with CO mixing ratios as shown in Fig. 3. The increase of $k_{OH}$ with CO was only partly due to the increase in reactivity from CO alone. Therefore, other reactants that were co-emitted with CO for example in combustion processes most likely contributed to the increase in reactivity. The correlation still holds, if only reactivity from OH reactants other than CO, $NO_x$ and isoprene is taken into account. This further supports that also OH reactivity from organic compounds is co-emitted with CO.

Back-trajectories were calculated for this campaign using the NOAA (Nation Oceanic and Atmospheric Administration) HYSPLIT (Hybrid Single Particle Lagrangian Integrated Trajectory Model) model (Stein et al., 2015), in order to test, if measured OH reactivities are correlated with the origin of advected air masses. 24-hour back-trajectories were calculated for air masses at the measurement site for each hour. During one day back-trajectories were typically very similar and therefore, trajectories shown in Fig. 4 are averages of trajectories calculated between 10:00 and 19:00. The majority of back-trajectories are pointing to locations south and less often to locations east or north of the measurement site. Mountains west and north of the measurements site appear as barriers for air masses. Only on three days (08, 27, 28 June) back-trajectories indicate that air masses originated from locations in the mountains north of the measurements site. Lowest $k_{OH}$ values ($< 10\,s^{-1}$) were observed in these cases due to less industry and less dense population in this area. In contrast, there is dense population in the sector from east to south of the measurements site. This likely explains why OH reactivity values were highest, if air masses were coming from this area. Also the correlation of $k_{OH}$ with CO as a proxy for the pick-up of emissions from anthropogenic activities is consistent with the origin of air masses.

The increase in OH reactivity during the first two weeks could be related to a change of the origin of air masses from the north (08 June) to the east (13 June) and finally to the south (15 June). However, no obvious difference of back-trajectories is seen before and after 20 June for similar origins of air masses, so that back-trajectories are not sufficient to explain, why measured OH reactivity would be generally higher and more spiky before 20 June.

The more likely reason are nearby emissions connected with harvesting of crop and combustion of straw and crop residuals on nearby agricultural fields in the first two weeks of June. On 13 June, for example, crop was harvested on the field directly next to the measurement place. Indicators for

Atmos. Chem. Phys. Discuss., doi:10.5194/acp-2016-716, 2016
Manuscript under review for journal Atmos. Chem. Phys.
Published: 10 August 2016


Atmospheric Chemistry and Physics Discussions

biomass burning activities were visually observed fires in surrounding areas, reduced visibility, and an increased load of measured particles. In addition, elevated concentrations of acetonitrile (a marker for biomass combustion) were measured between 12 and 19 June (Tan et al., 2016).

### 3.2 Contributions of OH reactants to the OH reactivity and missing reactivity

OH reactivity measurements are of particular value in order to test if all important OH reactants were detected. Volatile organic compounds (VOCs) and inorganic compounds such as nitrogen oxides ($NO_x$=NO+$NO_2$) and carbon monoxide (CO) are typically major contributors to the total OH reactivity. However, the number of OH reactants specifically of organic compounds is very large, so that a complete measurement is not necessarily expected. Therefore, comparison of direct $k_{OH}$ measurements with calculations from measured reactants can reveal unmeasured reactive compounds (missing reactivity) which present a gap in the constraints of model calculations used to test our knowledge of radical chemistry (Tan et al., 2016). In addition, VOCs and $NO_x$ concentrations are key species for understanding ozone formation, so that an incomplete knowledge of OH reactivity would lead to systematic errors in the calculation of photochemical ozone production.

The full time series of the calculated $k_{OH}$ is plotted together with the measured total $k_{OH}$ in Fig. 2.

Because of the similarity of diurnal profiles of observations during the first and the second part of the campaign, measured $k_{OH}$ and calculated reactivity from major contributors are shown as median diurnal profiles with percentiles in Fig. 5. Median diurnal profiles of all measured contributions are summed up and compared to measured $k_{OH}$ in Fig. 6. Ambient temperature was used for the calculation of reaction rate constants, but the differences between ambient temperature and the actual temperature in the instrument does not change any of the results shown here.

Overall, measured OH reactants can explain measured OH reactivity. The most important OH reactants were CO (on average 20 to 25 % of the total OH reactivity), nitrogen oxides (on average 12 to 22 % of the total OH reactivity) and OVOCs (on average 25 % of the total OH reactivity). Formaldehyde made the largest contribution to the reactivity from OVOCs (more than 50 %) and acetaldehyde the second largest contribution (20 to 25 %). The reactivity from isoprene makes a substantial contribution (often 20 %) to the total $k_{OH}$ in the afternoon. In contrast, reactivity from other measured OVOCs such as methanol, acetone and glyoxal made only small contributions to the OH reactivity. Reactivity from alkanes and alkenes were dominated by small alkenes mostly ethene and propene.

The median diurnal profile of the total OH reactivity had a maximum in the late night. It decreased during the day by nearly 50 % and started to increase after sunset. Accumulation of OH reactants during the night could be due to fresh emissions that are released into the shallow nocturnal boundary layer. A similar diurnal profile was also observed for contributions from $NO_x$, alkane and alkene species. Their concentrations are typically connected to emissions from anthropogenic activities. OH reactivity from $NO_x$ was also the largest contribution to $k_{OH}$ during night and early morning (20 to

Atmos. Chem. Phys. Discuss., doi:10.5194/acp-2016-716, 2016
Manuscript under review for journal Atmos. Chem. Phys.
Published: 10 August 2016


Atmospheric Chemistry and Physics Discussions

30 %). The diurnal profile of $NO_x$ appears as the major driver for the diurnal profile of the entire $k_{OH}$, whereas nearly all other contributions exhibited a less distinct diurnal profile. The opposite diurnal behavior than that for $NO_x$ was observed for isoprene, which is emitted by plants. The emission strength scales with light and temperature and, therefore, maximum mixing ratios were reached in the afternoon. The diurnal profile of isoprene counteracted partly the decrease of OH reactivity due to the decrease of $NO_x$, alkane and alkene species.

CO mixing ratios range between 300 and 1000 ppbv during this campaign. Therefore, reactivity from CO made always a large fraction of the total $k_{OH}$. The OH reactivity from CO showed only a weak diurnal profile with a median value of $3\,s^{-1}$ and could therefore be used as indicator for the overall origin of pollutants apart from diurnal changes. As discussed above, measured $k_{OH}$ scales with CO indicating that also co-emitted OH reactants such as alkenes were important (Fig. 3).

Only relatively few oxygenated volatile organic compounds (OVOCs) were measured in this campaign (Table 1). Nevertheless, their reactivity made a large fraction of the total reactivity with median values between 2 and $4\,s^{-1}$ over the course of one day. This was approximately one third of the total reactivity. Most of the reactivity from OVOC compounds were from formaldehyde and acetaldehyde. The good agreement between measured and calculated OH reactivity indicates that these were the most important organic oxidation products that contributed to the OH reactivity.

Similar to CO, there was only a weak diurnal profile of reactivity from OVOCs with decreasing values during the afternoon. This might be unexpected, because photochemistry that produces OVOCs is most active in the afternoon, so that OVOC species may accumulate. The higher concentrations could indicate that these OVOC species were regionally transported or were products from nighttime oxidation processes. Also direct emission of these species could explain such a diurnal profile, because concentrations would decrease, if the rise of the boundary layer height during morning hours diluted these species.

Although the general features of OH reactivity and OH reactants are similar during the entire campaign, there are also some differences. Measured OH reactivity was on average lower after 20 June specifically during the second half of the night and early morning, when median values were higher than $25\,s^{-1}$ before 20 June and 16 to $20\,s^{-1}$ later. Afternoon values were only slightly less after 20 June compared to the first part of the campaign. This is reflected in a decrease in median OH reactant concentrations during the second part of the campaign. It is most prominently seen in median alkene and alkane concentrations. In contrast, isoprene concentrations increased faster in the morning and high afternoon concentrations persisted in the evening during the second part of the campaign. Air temperatures were generally a few degree higher than during the first two weeks, so that temperature driven biogenic emissions could have been larger after 20 June. The largest fraction of higher OH reactivity observed in the first part of the campaign remains unexplained by OH reactant measurements.

Atmos. Chem. Phys. Discuss., doi:10.5194/acp-2016-716, 2016
Manuscript under review for journal Atmos. Chem. Phys.
Published: 10 August 2016


Atmospheric Chemistry and Physics Discussions

There is generally good agreement between the measured and calculated OH reactivity for most of the time (Fig. 2 and 6). Even during times, when measured reactivity is higher than calculations from OH reactants, the gap is only slightly larger than the combined $1\,\sigma$ uncertainties: The $k_{\mathrm{OH}}$ calculated from OH reactants has an uncertainty of $\pm 10\,\%$ to $\pm 15\,\%$ depending on the relative distributions of reactants and the measured $k_{\mathrm{OH}}$ has an uncertainty of maximum $\pm 10\,\%$ plus $\pm 0.7\,\mathrm{s}^{-1}$ ($1\sigma$ accuracies, Tab. 1).

Largest differences of 5 to $6\,\mathrm{s}^{-1}$ (approximately 20 %) occurred during nighttime and early morning during the first two weeks of the campaign, when also nitrogen oxide concentrations were highest. This could hint that unmeasured OH reactants were emitted concurrently with nitrogen oxides in combustion processes. Mainly the missing reactivity causes the higher measured OH reactivity in the first two weeks, whereas OH reactant concentrations (e. g. OVOCs) were only slightly higher.

Exceptionally good agreement is seen at nearly all times after 20 June in the time series as well as in the median diurnal profile (Fig. 2 and 6). Such good agreement is not necessarily expected due to the large number of possible OH reactants (Goldstein and Galbally, 2007). Specifically the number of OVOCs that were measured in this campaign is rather small and additional reactivity from other oxidation products could be expected to contribute to the total OH reactivity. The good agreement between measured and calculated $k_{\mathrm{OH}}$ indicates that other oxidation products than measured were not significantly contributing to the OH reactivity at the measurement site. One explanation could be that the photochemical age of air masses was short and therefore, oxidation products could not accumulate. This could be the case for fresh emissions close to the measurement site. On the other hand, loss rates of photochemically formed oxidation products may have been too short that they can accumulate due to for example deposition. In addition, the uncertainty of OH reactant measurements (up to 20 %) would allow that unmeasured oxidation products significantly contribute to the total OH reactivity.

### 3.3 Comparison with previous field campaigns

In our previous field campaigns in China 2006 in the Pearl-River-Delta, PRD, (Hofzumahaus et al., 2009; Lou et al., 2010; Lu et al., 2012) and Yufa close to Beijing (Lu et al., 2013), OH reactivity was considerably higher, but exhibited a similar diurnal profile. Maximum values were 40 to $50\,\mathrm{s}^{-1}$ in the night and early morning during the PRD and Yufa campaigns and reached minimum values around $20\,\mathrm{s}^{-1}$ in the afternoon. Absolute contributions from CO and $\mathrm{NO_x}$ were comparable with contributions in Wangdu 2014, with slightly higher CO concentrations in Yufa 2006. However, contributions from measured VOC were significantly higher in both previous campaigns compared to the Wangdu campaign in 2014 explaining partly the higher reactivity in these campaign.

In both previous campaigns, measurements of OVOCs were completely missing and the measured OH reactivity was found to be about two times larger than the total reactivity of measured CO, $\mathrm{NO_x}$ and hydrocarbons (Lou et al., 2010). The missing reactivity could be quantitatively explained by

Atmos. Chem. Phys. Discuss., doi:10.5194/acp-2016-716, 2016
Manuscript under review for journal Atmos. Chem. Phys.
Published: 10 August 2016


Atmospheric Chemistry and Physics Discussions

OVOCs which were simulated by a model from the photo-oxidation of the measured VOCs. The major modelled OVOCs were formaldehyde, acetaldehyde, MVK, MACR and some minor isoprene oxidation products, which together could explain 70 % of the missing reactivity (i.e., about one third of the total reactivity). In the Wangdu campaign, the calculated total OH reactivity was largely in agreement with the measured $k_{\mathrm{OH}}$. This time, formaldehyde, acetaldehyde, MVK, MACR and glyoxal were directly measured and accounted also for one third of the total reactivity. These species were also the most important OVOC species in other campaigns in anthropogenic dominated environments such as in Beijing (Shao et al., 2009), London (Whalley et al., 2016) and Tokyo (Yoshino et al., 2012). This confirms the high relevance of these specific carbonyl compounds as reactants for OH in the polluted boundary layer.

OH reactivity measurements in this campaign lie within the range of OH reactivity measurements during summertime at other locations that were mainly influenced by anthropogenic emissions like Nashville (Kovacs et al., 2003), New York (Ren et al., 2003), Houston (Mao et al., 2010) in the US, Tokyo in Japan (Chatani et al., 2009), Beijing (Williams et al., 2016) in China, and London (Whalley et al., 2016) in Great Britain. Also diurnal profiles of $k_{\mathrm{OH}}$ were similar in these campaigns with peak values between 15 and 50 $\mathrm{s}^{-1}$ in the early morning and minimum values in the afternoon. Like in this campaign, the shape of the diurnal profile was often determined by reactivity from nitrogen oxides. Care has to be taken, if missing reactivity is compared between different campaigns, because the number of measured OH reactants used to calculate the reactivity can significantly differ (Lou et al., 2010; Yang et al., 2016, and ref. therein). For the measurements in Beijing (Williams et al., 2016) approximately 25 % of the measured reactivity remained unexplained, although oxygenated organic species were partly measured. Approximately 30 % of the reactivity measured in Nashville could not be explained, even if modelled organic compounds were taken into account. For the other campaigns in anthropogenic influenced areas, measured OH reactivity could be explained by either measured OH reactants alone (London, New York, this campaign) or if in addition product species from model calculations were included (Yufa, PRD, Tokyo).

### 3.4 Experimental OH budget

OH reactivity measurements can be used not only to quantify the possible contribution of unmeasured OH reactants, but also allows quantification of the total OH production rate. Because OH is short-lived, it reaches a steady state within seconds. Thus, the total OH production rate ($P_{\mathrm{OH}}$) equals the total destruction rate ($D_{\mathrm{OH}}$). $D_{\mathrm{OH}}$ can be calculated as the product of $k_{\mathrm{OH}}$ and the OH concentration:

$$D_{\mathrm{OH}} = k_{\mathrm{OH}} \times [\mathrm{OH}] \quad (2)$$

This rate can be compared with the sum of production rates ($P_{\mathrm{OH}}$) from known OH sources. In this campaign, OH production from HONO and $O_3$ photolysis, ozonolysis of alkenes, and radical

Atmos. Chem. Phys. Discuss., doi:10.5194/acp-2016-716, 2016
Manuscript under review for journal Atmos. Chem. Phys.
Published: 10 August 2016


Atmospheric Chemistry and Physics Discussions

recycling reactions of $HO_2$ with NO and ozone can be calculated from measurements:

$$P_{OH} = P_{OH}(h\nu{+}O_3){+}P_{OH}(h\nu{+}HONO){+}P_{OH}(HO_2{+}O_3){+}P_{OH}(HO_2{+}NO){+}P_{OH}(O_3{+}alkene) \quad (3)$$

Potential, unknown OH sources can then be determined as the difference between $D_{OH}$ and $P_{OH}$. This was successfully applied for data from our previous field campaigns in China (Hofzumahaus et al., 2009) revealing significant unaccounted OH sources and in chamber studies (Fuchs et al., 2013, 2014; Nehr et al., 2014).

Time series of calculated OH production and destruction rates are plotted in Fig. 2 and median diurnal profiles of quantities that are required for this calculation in Fig. 7. Unfortunately, the data coverage of simultaneous measurements before 20 June is not sufficient to allow for an independent analysis of the first part of the campaign like for the analysis of OH reactants. However, results do not change significantly, whether the first part is included or not.

Figure 8 shows the median diurnal profile of the OH destruction and production rates and their difference including an estimate of the accuracy of the calculated difference. The diurnal profile of the OH production rate was mainly driven by solar radiation as expected from the photolytic nature of primary radical production, which also determines the overall abundance of $HO_2$. During daytime, the known OH production was dominated by the recycling reaction of $HO_2$ with NO reaching a maximum of about $10\,\mathrm{ppbv/h}$ shortly before noon. The relative contribution of primary OH production by either $O_3$ or HONO photolysis to the total OH production was increasing during the day to reach median maximum values of $1.2\,\mathrm{ppb/h}$ and $1.5\,\mathrm{ppb/h}$, respectively. The ozone photolysis exhibited a strong diurnal profile because both, solar radiation and ozone concentration had maximum vales at noon and early afternoon. An OH production rate from HONO photolysis of 1 to $1.5\,\mathrm{ppb/h}$ persisted into the afternoon due to relatively high HONO concentrations measured throughout the day. The budget of HONO will be discussed in a separate paper, but it is clear that HONO production from the reaction of OH with NO cannot explain the high HONO concentrations in the afternoon. Ozonolysis of alkene species made only a minor contribution to the OH production at all times.

The time series of the total OH production and destruction rates, determined by Eq. 2 and 3, respectively, were nearly balanced for most of the time (Fig. 2). The median diurnal profiles of $P_{OH}$ and $D_{OH}$ agree especially well in the morning (Fig. 8), whereas in the afternoon, the loss rate is slightly larger than the production rate. Although the difference is hardly significant with respect to the experimental accuracies (Fig. 8), a systematic trend with NO can be seen (Fig. 9).

For lowest NO mixing ratios of less than $0.3\,\mathrm{ppbv}$, OH destruction was nearly twice as large as the OH production, whereas production and destruction was balanced for NO mixing ratios higher than $1\,\mathrm{ppbv}$. This corresponds to the finding in Tan et al. (2016) that modelled OH tends to be smaller than measurements with decreasing NO during this campaign. A similar behavior was found in our

Atmos. Chem. Phys. Discuss., doi:10.5194/acp-2016-716, 2016
Manuscript under review for journal Atmos. Chem. Phys.
Published: 10 August 2016


Atmospheric Chemistry and Physics Discussions

previous field campaigns in China in 2006. However, the difference in the OH production and destruction was much larger and highly significant with respect to the experimental uncertainties of the calculated reaction rates (Hofzumahaus et al., 2009). The measured data of this campaign in Wangdu show the same tendency, but this time, the much weaker imbalance would also be explainable by the experimental errors of the chemical OH budget.

In addition to the measurement uncertainties stated in Tab. 1, instrumental tests during this campaign cannot exclude that OH concentration measurements are partly affected by an artifact as discussed in detail in Tan et al. (2016). The upper limit for an instrumental interference was estimated to be equivalent to an OH concentration of $1 \times 10^6\,\mathrm{cm}^{-3}$. This positive bias would also give a positive bias in the calculated OH destruction rate.

In the night, OH production from sources taken into account in this calculation is close to zero because there is no radiation. This suppresses both OH production from photolysis reactions and OH regeneration by the reaction of peroxy radicals with NO that is mainly formed from $NO_2$ photolysis. Because of the relatively high OH reactivity OH concentrations are expected to be very small. However, median measured OH concentrations ranged between 0.5 to $1 \times 10^6\,\mathrm{cm}^{-3}$ (Fig. 7). A median OH production of 1 to $2\,\mathrm{ppbv/h}$ would be required to explain measured nighttime OH concentrations (Fig. 8).

Potential reasons for additional OH production at night have been recently discussed by Lu et al. (2014), such as OH production by ozonolysis of terpenoids or dissociation of radical reservoir species like PAN that may be transported downward in the nocturnal boundary layer. Such mechanisms may have played a role at Wangdu, but we have no suitable measured data to test these hypothesis.

However, the impact of a potential interference in the OH concentration measurements would also be largest in the night (Fig. 8), because nearly the entire OH signal could be due to interferences. As a consequence, the difference between calculated OH production and destruction during nighttime is within this additional uncertainty. The calculated OH destruction rate is less affected during daytime, when a potential OH interference of less than $1 \times 10^6\,\mathrm{cm}^{-3}$ would only be a small fraction of the total measured OH (Tan et al., 2016).

In our previous field campaigns in China 2006, the OH turnover rate was significantly higher than in this campaign. In PRD and Yufa, maximum mean turnover rates (OH destruction rates) of $40\,\mathrm{ppbv/h}$ and $20\,\mathrm{ppbv/h}$, respectively, were reached around noontime (Lu et al., 2012, 2013). These values are 1.5 to 3 times higher than median OH turnover rates in this campaign. As discussed above, the major difference is that measured OH reactivities were significantly higher in the previous campaigns. The resulting higher loss rate was only partly balanced by a higher OH production from the reaction of $HO_2$ with NO, which was nearly a factor two larger in PRD and Yufa. Therefore, also the gap between calculated OH destruction and production was clearly above the level of significance (Hofzumahaus et al., 2009).

Atmos. Chem. Phys. Discuss., doi:10.5194/acp-2016-716, 2016
Manuscript under review for journal Atmos. Chem. Phys.
Published: 10 August 2016


Atmospheric Chemistry and Physics Discussions

Also the distribution of primary OH sources is different in this campaign compared to our previous campaigns in China, when HONO photolysis exhibited a diurnal profile with maximum values in the morning. These values were larger compared to this campaign, but HONO mixing ratios dropped to lower values in the afternoon, so that production by HONO photolysis was less in Yufa and PRD than in Wangdu 2016. Nevertheless, total primary OH production was higher (factor of 2 in PRD and factor of 1.5 in Yufa) in the previous campaigns.

HONO photolysis was also the most important primary source for OH radicals in other campaigns that were conducted in anthropogenic dominated environments for example in New York (Ren et al., 2003), in Paris (Michoud et al., 2012), Mexico City (Dusanter et al., 2009), Santiago (Elshorbany et al., 2009), and Tokyo (Kanaya et al., 2007). These campaigns took place in or very close to very large cities and NO concentrations were often exceptionally high, so that HONO formation was favored. Our measurement site in Wangdu was not directly located in an urban area and therefore the $NO_x$ concentrations were only moderately high in the morning and rather small in the afternoon, so that the importance of HONO as largest primary source for OH was not necessarily expected.

## 4 Summary and conclusions

OH reactivity was measured during a comprehensive field campaign at Wangdu in summer 2014. Additional measurements of OH reactants, OH concentrations and quantities that are required to calculate OH production ($HO_2$, NO $O_3$, HONO, photolysis frequencies) allowed comparing OH reactivity measurements with calculations from measured OH reactants and analyzing the chemical OH budget from measurements alone.

Overall, measured OH reactivity can mostly be explained by OH reactants measurements, specifically during the second half of the campaign. The diurnal profile of OH reactivity, the distribution of OH reactants and the good correlation of the OH reactivity with CO indicates that the chemical composition at the measurement site was mainly impacted by anthropogenic emissions. In our previous field campaigns in China 2006, the number of OH reactants that were measured was less and, thus, only approximately 50 % of the measured OH reactivity was explained by measured OH reactants (Lou et al., 2010; Lu et al., 2012, 2013). However, additional OH reactants determined by model calculations could close the gap in these cases. In this campaign, the good agreement between measured and calculated reactivity indicates that all important organic compounds were measured including oxidation products.

OH production and destruction were mainly balanced within the uncertainty of measurements. The accuracy of this calculation was lowered by additional uncertainty in the OH concentration measurements due to a potential bias (Tan et al., 2016). Despite this uncertainty, the OH destruction tends to be higher than OH production in the late afternoon, when NO concentrations were lowest.

Atmos. Chem. Phys. Discuss., doi:10.5194/acp-2016-716, 2016
Manuscript under review for journal Atmos. Chem. Phys.
Published: 10 August 2016


Atmospheric Chemistry and Physics Discussions

This result is consistent with the analysis of model calculations (Tan et al., 2016) and findings in previous field campaigns (Hofzumahaus et al., 2009).

However, in 2006 the observed discrepancy between the OH production and destruction rates was significantly larger requiring an additional OH source to close the gap. The major difference to this campaign was that the measured OH reactivity was much higher. Therefore, a significant gap in OH production and destruction rates were found in contrast to results in this campaign.

*Acknowledgements.* We thank the science teams of Wangdu-2014 campaign. This work was supported by the National Natural Science Foundation of China (Major Program: 21190052 and Innovative Research Group: 41121004), the Strategic Priority Research Program of the Chinese Academy of Sciences (grant no. XDB05010500), the Collaborative Innovation Center for Regional Environmental Quality, and by the EU-project AMIS (Fate and Impact of Atmospheric Pollutants, PIRSES-GA-2011-295132). The authors gratefully acknowledge the NOAA Air Resources Laboratory (ARL) for the provision of the HYSPLIT transport and dispersion model and/or READY website (http://www.ready.noaa.gov) used in this publication.

Atmos. Chem. Phys. Discuss., doi:10.5194/acp-2016-716, 2016
Manuscript under review for journal Atmos. Chem. Phys.
Published: 10 August 2016


Atmospheric Chemistry and Physics Discussions

## References


Chatani, S., Shimo, N., Matsunaga, S., Kajii, Y., Kato, S., Nakashima, Y., Miyazaki, K., Ishii, K., and Ueno, H.: Sensitivity analyses of OH missing sinks over Tokyo metropolitan area in the summer of 2007, Atmos. Chem. Phys., 9, 8975–8986, doi:10.5194/acp-9-8975-2009, 2009.

Dusanter, S., Vimal, D., Stevens, P. S., Volkamer, R., Molina, L. T., Baker, A., Meinardi, S., Blake, D., Sheehy, P., Merten, A., Zhang, R., Zheng, J., Fortner, E. C., Junkermann, W., Dubey, M., Rahn, T., Eichinger, B., Lewandowski, P., Prueger, J., and Holder, H.: Measurements of OH and $HO_2$ concentrations during the MCMA-2006 field campaign - Part 2: Model comparison and radical budget, Atmos. Chem. Phys., 9, 6655–6675, doi:10.5194/acp-9-6655-2009, 2009.

Ehhalt, D. H.: Photooxidation of trace gases in the troposphere, Phys. Chem. Chem. Phys., 1, 5401–5408, doi:10.1039/a905097c, 1999.

Elshorbany, Y. F., Kurtenbach, R., Wiesen, P., Lissi, E., Rubio, M., Villena, G., Gramsch, E., Rickard, A. R., Pilling, M. J., and Kleffmann, J.: Oxidation capacity of the city air of Santiago, Chile, Atmos. Chem. Phys., 2009, 2257–2273, doi:10.5194/acp-9-2257-2009, 2009.

Fuchs, H., Bohn, B., Hofzumahaus, A., Holland, F., Lu, K. D., Nehr, S., Rohrer, F., and Wahner, A.: Detection of $HO_2$ by laser-induced fluorescence: calibration and interferences from $RO_2$ radicals, Atmos. Meas. Tech., 4, 1209–1255, doi:10.5194/amt-4-1209-2011, 2011.

Fuchs, H., Hofzumahaus, A., Rohrer, F., Bohn, B., Brauers, T., Dorn, H.-P., Häseler, R., Holland, F., Kaminski, M., Li, X., Lu, K., Nehr, S., Tillmann, R., Wegener, R., and Wahner, A.: Experimental evidence for efficient hydroxyl radical regeneration in isoprene oxidation, Nature Geosci., 6, 1023–1026, doi:10.1038/NGEO1964, 2013.

Fuchs, H., Acir, I. H., Bohn, B., Brauers, T., Dorn, H. P., Häseler, R., Hofzumahaus, A., Holland, F., Kaminski, M., Li, X., Lu, K., Lutz, A., Nehr, S., Rohrer, F., Tillmann, R., Wegener, R., and Wahner, A.: OH regeneration from methacrolein oxidation investigated in the atmosphere simulation chamber SAPHIR, Atmos. Chem. Phys., 14, 7895–7908, doi:10.5194/acp-14-7895-2014, 2014.

Goldstein, A. H. and Galbally, I. E.: Known and unexplored organic constituents in the earth's atmosphere, Environ. Sci. Technol., 41, 1514–1521, doi:10.1021/es072476p, 2007.

Hofzumahaus, A., Rohrer, F., Lu, K., Bohn, B., Brauers, T., Chang, C.-C., Fuchs, H., Holland, F., Kita, K., Kondo, Y., Li, X., Lou, S., Shao, M., Zeng, L., Wahner, A., and Zhang, Y.: Amplified trace gas removal in the troposphere, Science, 324, 1702–1704, doi:10.1126/science.1164566, 2009.

Holland, F., Hofzumahaus, A., Schäfer, J., Kraus, A., and Pätz, H. W.: Measurements of OH and $HO_2$ radical concentrations and photolysis frequencies during BERLIOZ, J. Geophys. Res., 108, 8246, doi:10.1029/2001JD001393, 2003.

Kanaya, Y., Cao, R., Akimoto, H., Fukuda, M., Komazaki, Y., Yokouchi, Y., Koike, M., Tanimoto, H., Takegawa, N., and Kondo, Y.: Urban photochemistry in central Tokyo: 1. observed and modeled OH and $HO_2$ radical concentrations during the winter and summer 2004, doi:10.1029/2007JD008670, 2007.

Kovacs, T. A., Brune, W. H., Harder, H., Martinez, M., Simpas, J. B., Frost, G. J., Williams, E., Jobson, T., Stroud, C., Young, V., Fried, A., and Wert, B.: Direct measurements of urban OH reactivity during Nashville SOS in summer 1999, J. Environ. Monit., 5, 68–74, doi:10.1039/B204339D, 2003.

Atmos. Chem. Phys. Discuss., doi:10.5194/acp-2016-716, 2016
Manuscript under review for journal Atmos. Chem. Phys.
Published: 10 August 2016




Li, X., Rohrer, F., Hofzumahaus, A., Brauers, T., Häseler, R., Bohn, B., Broch, S., Fuchs, H., Gomm, S., Holland, F., Jäger, J., Kaiser, J., Keutsch, F. N., Lohse, I., Lu, K., Tillmann, R., Wegener, R., Wolfe, G. M., Mentel, T. F., Kiendler-Scharr, A., and Wahner, A.: Missing gas-phase source of HONO inferred from Zeppelin measurements in the troposphere, Science, 344, 292–296, doi:10.1126/science.1248999, 2014.

Lou, S., Holland, F., Rohrer, F., Lu, K., Bohn, B., Brauers, T., Chang, C. C., Fuchs, H., Häseler, R., Kita, K., Kondo, Y., Li, X., Shao, M., Zeng, L., Wahner, A., Zhang, Y., Wang, W., and Hofzumahaus, A.: Atmospheric OH reactivities in the Pearl River Delta - China in summer 2006: measurement and model results, Atmos. Chem. Phys., 10, 11 243–11 260, doi:10.5194/acp-10-11243-2010, 2010.

Lu, K., Zhang, Y., Su, H., Brauers, T., Chou, C. C., Hofzumahaus, A., Liu, S. C., Kita, K., Kondo, Y., Shao, M., Wahner, A., Wang, J., Wang, X., and Zhu, T.: Oxidant ($O_3$ + $NO_2$) production processes and formation regimes in Beijing, J. Geophys. Res., 115, D07 303, doi:10.1029/2009JD012714, 2010.

Lu, K. D., Rohrer, F., Holland, F., Fuchs, H., Bohn, B., Brauers, T., Chang, C. C., Häseler, R., Hu, M., Kita, K., Kondo, Y., Li, X., Lou, S. R., Nehr, S., Shao, M., Zeng, L. M., Wahner, A., Zhang, Y. H., and Hofzumahaus, A.: Observation and modelling of OH and $HO_2$ concentrations in the Pearl River Delta 2006: a missing OH source in a VOC rich atmosphere, Atmos. Chem. Phys., 12, 1541–1569, doi:10.5194/acp-12-1541-2012, 2012.

Lu, K. D., Hofzumahaus, A., Holland, F., Bohn, B., Brauers, T., Fuchs, H., Hu, M., Häseler, R., Kita, K., Kondo, Y., Li, X., Lou, S. R., Oebel, A., Shao, M., Zeng, L. M., Wahner, A., Zhu, T., Zhang, Y. H., and Rohrer, F.: Missing OH source in a suburban environment near Beijing: observed and modelled OH and $HO_2$ concentrations in summer 2006, Atmos. Chem. Phys., 13, 1057–1080, doi:10.5194/acp-13-1057-2013, 2013.

Lu, K. D., Rohrer, F., Holland, F., Fuchs, H., Brauers, T., Oebel, A., Dlugi, R., Hu, M., Li, X., Lou, S. R., Shao, M., Zhu, T., Wahner, A., Zhang, Y. H., and Hofzumahaus, A.: Nighttime observation and chemistry of $HO_X$ in the Pearl River Delta and Beijing in summer 2006, Atmos. Chem. Phys., 14, 4979–4999, doi:10.5194/acp-14-4979-2014, 2014.

Mao, J., Ren, X., Chen, S., Brune, W. H., Chen, Z., Martinez, M., Harder, H., Lefer, B., Rappenglück, B., Flynn, J., and Leuchner, M.: Atmospheric oxidation capacity in the summer of Houston 2006: Comparison with summer measurements in other metropolitan studies, Atmos. Environ., 44, 4107–4115, doi:10.1016/j.atmosenv.2009.01.013, 2010.

Michoud, V., Kukui, A., Camredon, M., Colomb, A., Borbon, A., Miet, K., Aumont, B., Beekmann, M., Durand-Jolibois, R., Perrier, S., Zapf, P., Siour, G., Ait-Helal, W., Locoge, N., Sauvage, S., Afif, C., Gros, V., Furger, M., Ancellet, G., and Doussin, J. F.: Radical budget analysis in a suburban European site during the MEGAPOLI summer field campaign, Atmos. Chem. Phys., 12, 11 951–11 974, doi:10.5194/acp-12-11951-2012, 2012.

Min, K. E., Washenfelder, R. A., Dube, W. P., Langford, A. O., Edwards, P. M., Zarzana, K. J., Stutz, J., Lu, K., Rohrer, F., Zhang, Y., and Brown, S. S.: A broadband cavity enhanced absorption spectrometer for aircraft measurements of glyoxal, methylglyoxal, nitrous acid, nitrogen dioxide, and water vapor, Atmos. Meas. Tech., 9, 423–440, doi:10.5194/amt-9-423-2016, 2016.



Nehr, S., Bohn, B., Dorn, H. P., Fuchs, H., Häseler, R., Hofzumahaus, A., Li, X., Rohrer, F., Tillmann, R., and Wahner, A.: Atmospheric photochemistry of aromatic hydrocarbons: OH budgets during SAPHIR chamber experiments, Atmos. Chem. Phys., 14, 6941–6952, doi:10.5194/acp-14-6941-2014, 2014.

Parker, A. E., Amedro, D., Schoemaecker, C., and Fittschen, C.: OH radical reactivity measurements by FAGE, Environ. Engin. Manag. J., 10, 107–114, 2011.

Ren, X., Harder, H., Martinez, M., Lesher, R. L., Oliger, A., Shirley, T., Adams, J., Simpas, J. B., and Brune, W. H.: $HO_X$ concentrations and OH reactivity observations in New York City during PMTACS-NY2001, Atmos. Environ., 37, 3627–3637, 2003.

Rohrer, F., Lu, K., Hofzumahaus, A., Bohn, B., Brauers, T., Chang, C.-C., Fuchs, H., Haseler, R., Holland, F., Hu, M., Kita, K., Kondo, Y., Li, X., Lou, S., Oebel, A., Shao, M., Zeng, L., Zhu, T., Zhang, Y., and Wahner, A.: Maximum efficiency in the hydroxyl-radical-based self-cleansing of the troposphere, Nature Geosci., 7, 559–563, doi:10.1038/ngeo2199, 2014.

Sadanaga, Y., Yoshino, A., Watanaba, K., Yoshioka, A., Wakazono, Y., Kanaya, Y., and Kajii, Y.: Development of a measurement system of peroxy radicals using a chemical amplification/laser-induced fluorescence technique, Rev. Sci. Instrum., 75, 864–872, doi:10.1063/1.1666985, 2004.

Shao, M., Lu, S., Liu, Y., Xie, X., Chang, C., Huang, S., and Chen, Z.: Volatile organic compounds measured in summer in Beijing and their role in ground-level ozone formation, J. Geophys. Res., 114, doi:10.1029/2008JD010863, 2009.

Stein, A. F., Draxler, R. R., Rolph, G. D., Stunder, B. J. B., Cohen, M. D., and Ngan, F.: NOAA's HYSPLIT atmospheric transport and dispersion modeling system, Bulletin of the American Meteorological Society, 96, 2059–2077, doi:10.1175/BAMS-D-14-00110.1, 2015.

Stone, D., Whalley, L. K., Ingham, T., Edwards, P. M., Cryer, D. R., Brumby, C. A., Seakins, P. W., and Heard, D. E.: Measurement of OH reactivity by laser flash photolysis coupled with laser-induced fluorescence spectroscopy, Atmos. Meas. Tech. Discuss., 2016, 1–22, doi:10.5194/amt-2016-51, 2016.

Tan, Z., Fuchs, H., Lu, K., Bohn, B., Broch, S., Gomm, S., Häseler, R., Hofzumahaus, A., Holland, F., Huang, X., Li, X., Liu, Y., Rohrer, F., Shao, M., Wang, B., Wang, M., Wu, Y., Wahner, A., and Zhang, Y.: Radical chemistry at a rural site (Wangdu) in the North China Plain: Observation and model calculations of OH, $HO_2$ and $RO_2$ radicals, Atmos. Chem. Phys. Discuss., 16, submitted, 2016.

Wang, M., Zeng, L., Lu, S., Shao, M., Liu, X., Yu, X., Chen, W., Yuan, B., Zhang, Q., Hu, M., and Zhang, Z.: Development and validation of a cryogen-free automatic gas chromatograph system (GC-MS/FID) for online measurements of volatile organic compounds, Analytical Methods, 6, 9424–9434, doi:10.1039/C4AY01855A, 2014.

Whalley, L. K., Stone, D., Bandy, B., Dunmore, R., Hamilton, J. F., Hopkins, J., Lee, J. D., Lewis, A. C., and Heard, D. E.: Atmospheric OH reactivity in central London: observations, model predictions and estimates of in situ ozone production, Atmos. Chem. Phys., 16, 2109–2122, doi:10.5194/acp-16-2109-2016, 2016.

Williams, J., Kessel, S. U., Nolscher, A. C., Yang, Y., Lee, Y., Yanez-Serrano, A. M., Wolff, S., Kesselmeier, J., Klupfel, T., Lelieveld, J., and Shao, M.: Opposite OH reactivity and ozone cycles in the Amazon rainforest and megacity Beijing: Subversion of biospheric oxidant control by anthropogenic emissions, Atmos. Environ., 125, Part A, 112–118, doi:10.1016/j.atmosenv.2015.11.007, 2016.

Atmos. Chem. Phys. Discuss., doi:10.5194/acp-2016-716, 2016
Manuscript under review for journal Atmos. Chem. Phys.
Published: 10 August 2016


Atmospheric Chemistry and Physics Discussions

610 Yang, Y., Shao, M., Wang, X., Nölscher, A. C., Kessel, S., Guenther, A., and Williams, J.: Towards a quantitative understanding of total OH reactivity: A review, Atmos. Environ., 134, 147–161, doi:10.1016/j.atmosenv.2016.03.010, 2016.

Yoshino, A., Nakashima, Y., Miyazaki, K., Kato, S., Suthawaree, J., Shimo, N., Matsunaga, S., Chatani, S., Apel, E., Greenberg, J., Guenther, A., Ueno, H., Sasaki, H., Hoshi, J.-y., Yokota, H., Ishii, K., and Kajii, Y.:
615 Air quality diagnosis from comprehensive observations of total OH reactivity and reactive trace species in urban central Tokyo, Atmospheric Environment, doi:10.1016/j.atmosenv.2011.12.029, 2012.

Atmos. Chem. Phys. Discuss., doi:10.5194/acp-2016-716, 2016
Manuscript under review for journal Atmos. Chem. Phys.
Published: 10 August 2016


Atmospheric Chemistry and Physics Discussions

**Table 1.** Instruments deployed in the campaign and used for data analysis.

| | measurement technique | time resolution | 1 $\sigma$ detection limit | 1 $\sigma$ accuracy |
|---|---|---|---|---|
| $k_{OH}$ | LP-LIF [a] | 180 s | 0.3 $s^{-1}$ | ±10 % ±0.7 $s^{-1}$ |
| OH | LIF [b] | 32 s | 0.32 $\times 10^6$ $cm^{-3}$ | ±11 % |
| $HO_2$ | LIF [b] | 32 s | 0.10 $\times 10^8$ $cm^{-3}$ | ±16 % |
| photolysis frequency | spectroradiometer | 20 s | [c] | ±10 % |
| $O_3$ | UV photometry | 60 s | 0.5 ppbv | ±5 % |
| NO | chemiluminescence | 180 s | 60 pptv | ±20 % |
| $NO_2$ | chemiluminescence[d] | 600 s | 300 pptv | ±20 % |
| HONO | LOPAP[e] | 300 s | 7 pptv | ±20 % |
| CO, $CH_4$, $CO_2$, $H_2O$ | cavity ring down | 60 s | [f] | [g] |
| $SO_2$ | pulsed UV fluorescence | 60 s | 0.1 ppbv | ±5 % |
| HCHO | Hantzsch fluorimetry | 60 s | 25 pptv | ±5 % |
| volatile organic compounds[h] | GC-FID/MS [l] | 1 h | 20 to 300 pptv | ±15 to 20 % |
| volatile organic compounds[i] | PTR-MS | 20 s | 0.2 ppbv | ±15 % |
| glyoxal | CEAS[j] | 1 s | 0.02 ppbv | ±5.8 % |

[a] laser photolysis - laser induced fluorescence
[b] laser induced fluorescence
[c] process specific, 5 order of magnitudes lower than maximum in noon time
[d] photolytical conversion to NO before detection, home built converter
[e] long-path absorption photometry
[f] species specific, for CO: 1 ppbv; $CH_4$:1 ppbv; $CO_2$: 25 ppbv; $H_2O$: 0.1 % (absolute water vapor content);
[g] species specific, for CO: 1 ppbv; $CH_4$:±1 ppbv; $CO_2$: ±25 ppbv; $H_2O$: ±5 %
[h] VOCs including $C_2$-$C_{11}$ alkanes, $C_2$-$C_6$ alkenes, $C_6$-$C_{10}$ aromatics
[i] OVOCs including acetaldehyde, methyl-vinyl ketone and methacrolein
[j] cavity-enhanced-absorption spectroscopy

Atmos. Chem. Phys. Discuss., doi:10.5194/acp-2016-716, 2016
Manuscript under review for journal Atmos. Chem. Phys.
Published: 10 August 2016


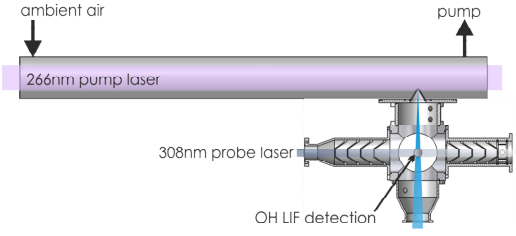


**Figure 1.** Schematics of the Jülich OH reactivity instrument. Ambient air is sampled into a flow tube. A small part of the air is drawn into the OH detection cell that is operated at a pressure of 4 hPa. High OH concentrations are produced by flash photolysis of ozone at 266 nm at a low frequency of 1 to 2 Hz. The OH concentration is probed at a high frequency of 8.5 kHz, so that the loss of OH radicals due to their reaction with OH reactants in the ambient air can be observed.

Atmos. Chem. Phys. Discuss., doi:10.5194/acp-2016-716, 2016
Manuscript under review for journal Atmos. Chem. Phys.
Published: 10 August 2016


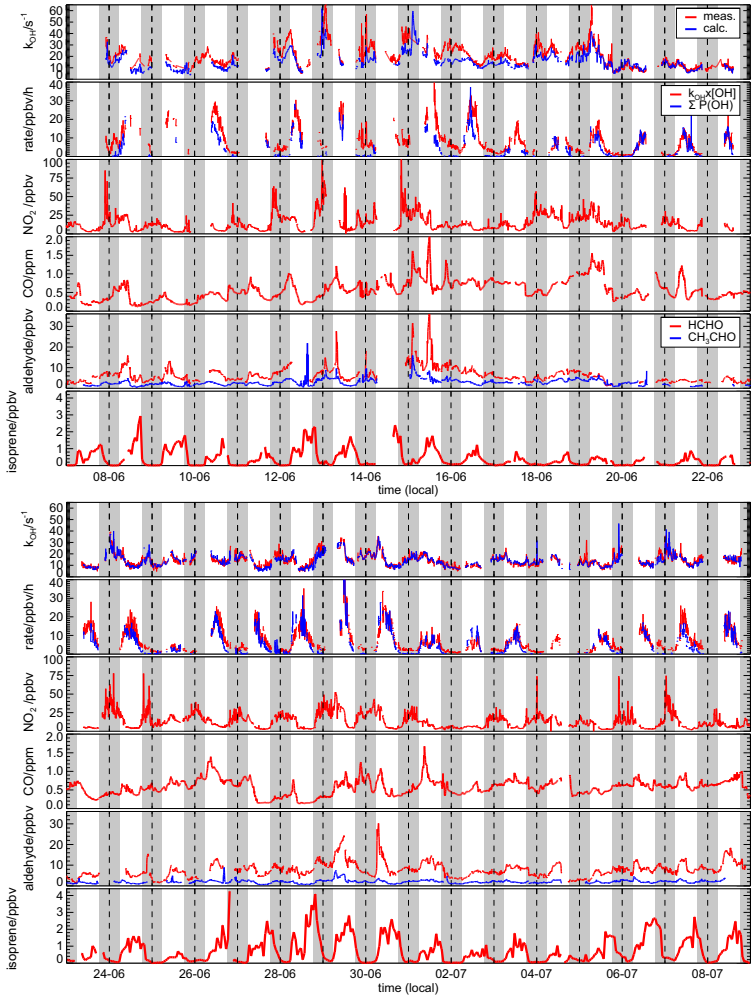


**Figure 2.** Time series of measured and calculated OH reactivity. In addition, time series of the OH destruction rate ($D_{\mathrm{OH}}$) calculated from measured OH concentrations and OH reactivity is shown together with the sum of measured OH production rates ($\sum P_{\mathrm{OH}}$) from $O_3$ and HONO photolysis and reactions of $HO_2$ with NO and $O_3$. Lower panels give time series of important trace gas measurements contributing to the OH reactivity.

Atmos. Chem. Phys. Discuss., doi:10.5194/acp-2016-716, 2016
Manuscript under review for journal Atmos. Chem. Phys.
Published: 10 August 2016


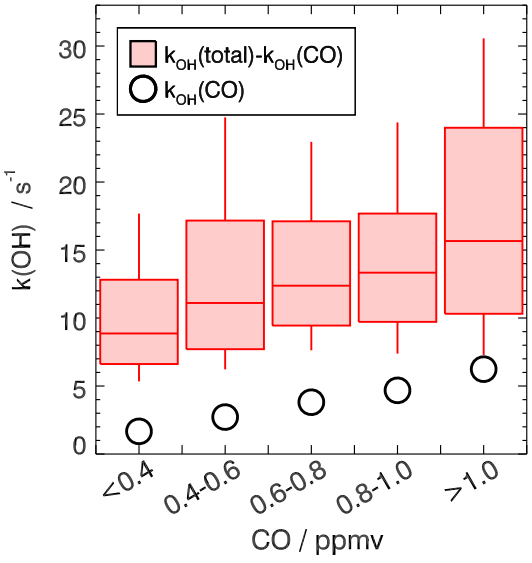


**Figure 3.** Correlation between OH reactivity excluding CO and CO mixing ratios. Red boxes give 25 and 75 percentiles and whiskers 10 and 90 percentiles of the $k_{\mathrm{OH}}$ distribution. Black circles show median values of OH reactivity that is in addition caused by CO.

Atmos. Chem. Phys. Discuss., doi:10.5194/acp-2016-716, 2016
Manuscript under review for journal Atmos. Chem. Phys.
Published: 10 August 2016


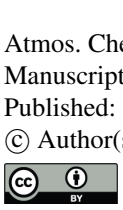

Atmospheric Chemistry and Physics Discussions

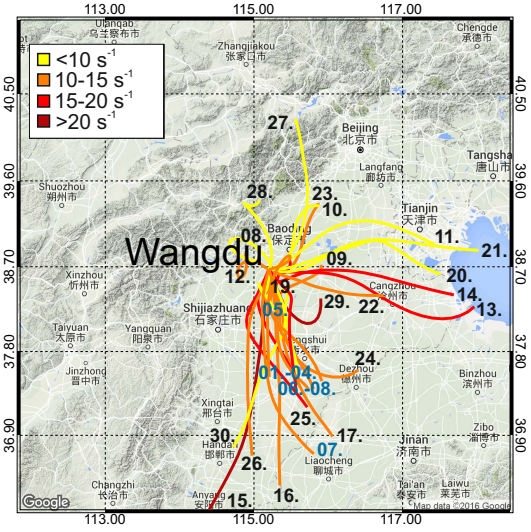


**Figure 4.** NOAA Hysplit 24-hour back-trajectories during the campaign calculated as averages of hourly back-trajectories between 10:00 and 19:00 local time. Colors of trajectories indicate the OH reactivity level measured at the field site in Wangdu. Black numbers indicate the date in June, dark blue numbers the date in July.

Atmos. Chem. Phys. Discuss., doi:10.5194/acp-2016-716, 2016
Manuscript under review for journal Atmos. Chem. Phys.
Published: 10 August 2016


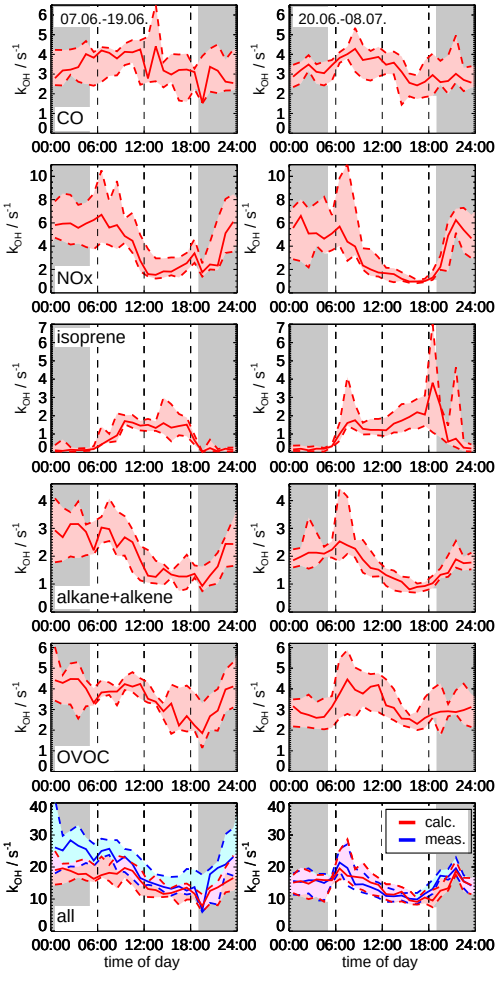


**Figure 5.** Median diurnal profiles of reactivity from major measured OH reactants and of the total measured and calculated OH reactivity for the first and second part of the campaign. Data is only included, if all major OH reactants and OH reactivity were concurrently measured. Colored areas give 25 and 75 percentiles.

Atmos. Chem. Phys. Discuss., doi:10.5194/acp-2016-716, 2016
Manuscript under review for journal Atmos. Chem. Phys.
Published: 10 August 2016


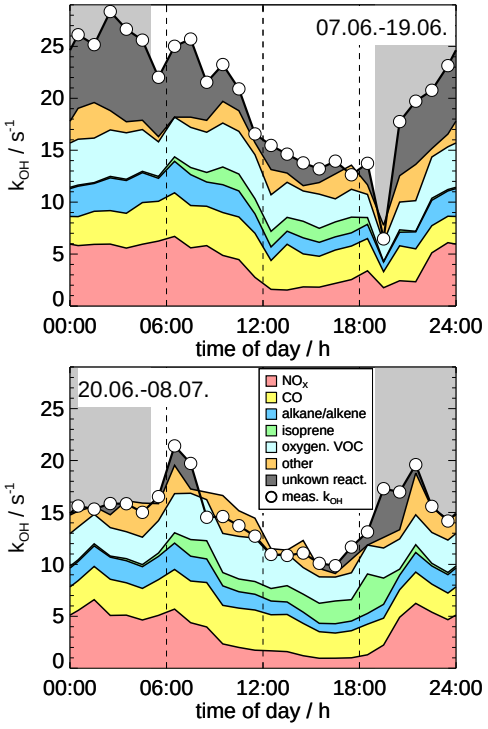


**Figure 6.** Sum of median diurnal profiles of reactivities from all measured OH reactants compared to the measured OH reactivity for the first and second part of the campaign. Data is only included, if all major OH reactants and OH reactivity were concurrently measured. "Other" include small contributions from measured OH reactants listed in Table 1 that are not included in the other groups. The dark grey area indicates missing OH reactivity from unmeasured OH reactants.

Atmos. Chem. Phys. Discuss., doi:10.5194/acp-2016-716, 2016
Manuscript under review for journal Atmos. Chem. Phys.
Published: 10 August 2016


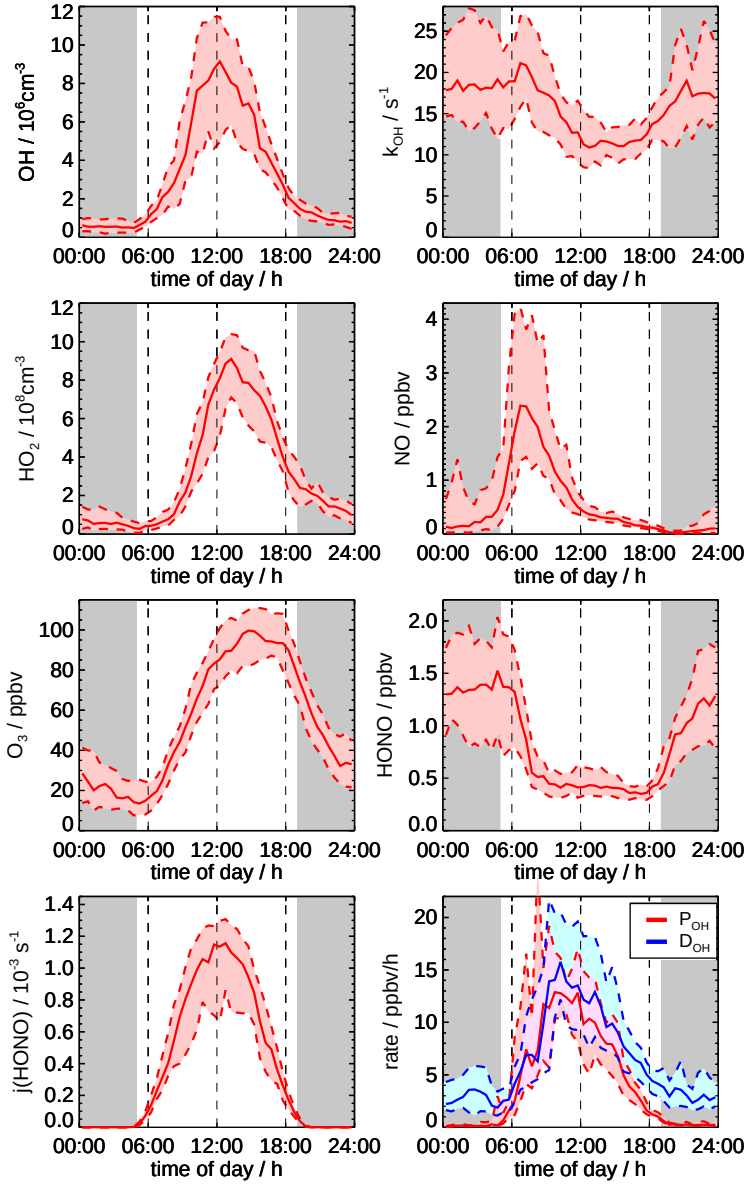


**Figure 7.** Median diurnal profiles of trace gas concentrations used for the calculation of the total OH production rate ($P_{\mathrm{OH}}$) and destruction rate ($D_{\mathrm{OH}}$). Data is only included, if all required trace gas concentrations and OH reactivity were concurrently measured. Colored areas give 25 and 75 percentiles.

Atmos. Chem. Phys. Discuss., doi:10.5194/acp-2016-716, 2016
Manuscript under review for journal Atmos. Chem. Phys.
Published: 10 August 2016


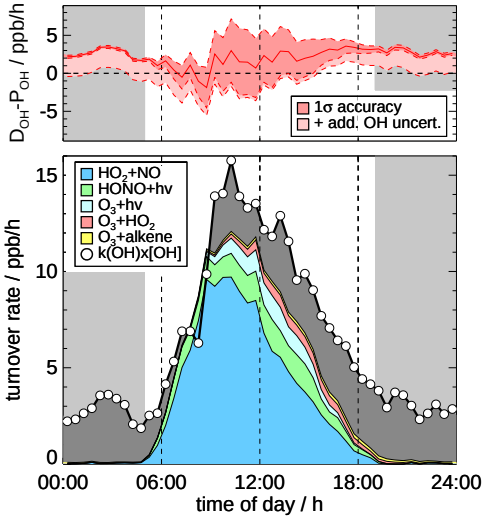


**Figure 8.** Median diurnal profiles of OH production ($P_{\mathrm{OH}}$) and destruction ($D_{\mathrm{OH}}$) rates. Data is only included, if all required trace gas concentrations and OH reactivity were concurrently measured. Dark grey areas indicate missing OH production. The upper panel gives the 1 $\sigma$ accuracy of the difference ($D_{\mathrm{OH}}$- $P_{\mathrm{OH}}$) calculated from the uncertainties of measurements (Gaussian error propagation). The effect on the accuracy from an upper limit of potential interferences in the OH measurements is shown separately.

Atmos. Chem. Phys. Discuss., doi:10.5194/acp-2016-716, 2016
Manuscript under review for journal Atmos. Chem. Phys.
Published: 10 August 2016


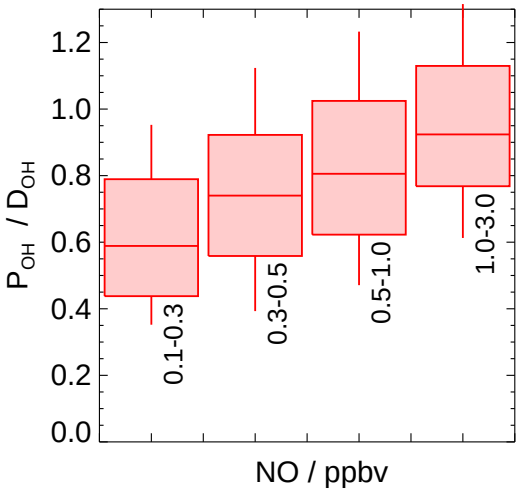


**Figure 9.** Box and whisker plot of the ratio of the total OH production ($P_{\mathrm{OH}}$) and the OH destruction rate ($D_{\mathrm{OH}}$) as a function of the NO mixing ratio for daytime values. Boxes give 25 and 75 percentiles and whiskers 10 and 90 percentiles. Data is only included, if all required trace gas concentrations and OH reactivity were concurrently measured.